Simulating Prosthetic Devices with Human-Inspired Hybrid Control

Ryan W. Sinnet, Huihua Zhao, and Aaron D. Ames

***Abstract*— A method is proposed which enables testing of prosthetic devices in simulation. A hybrid model is used to represent human walking—the combination of continuous and discrete dynamics motivates the use of hybrid systems. A human walking experiment is analyzed and mathematical functions on the kinematics of the collected data are found which capture some of the fundamental behaviors associated with human walking. One model is considered in which these behaviors are fully tracked using feedback linearization; the intent of this is to simulate healthy human walking. Then, a second model is considered: this model is assumed to be a human with a transfemoral prosthesis; PD control is used on the prosthesis. All models considered demonstrate locally exponentially stable periodic orbits when simulated for four separate test subjects, or, in other words, the models exhibit stable walking even with a prosthetic lower extremity. The methods used in this paper are a stepping stone toward a process capable of rapidly prototyping potential prosthesis designs and controllers.**

I. INTRODUCTION

As of 2002, there are approximately 1.4 million people living in the United States with an amputated lower extremity. Approximately 350,000 of these people have a transfemoral amputation [1]. The sheer numbers motivate research into intelligent prosthetics. While the concept of prosthetics has been around for a long time [2], a paradigm shift occurred when researchers started exploring the idea of *intelligent* or *controlled prosthetics*. By outfitting a prosthetic leg with a motor and some type of controller, the potential for a more efficient prosthesis is created; indeed, research exists regarding the efficiency of such prostheses [3], [4]. Considering the number of parameters associated with designing a prosthesis (physical parameters, controllers/gains, etc.), one quickly sees the need for a way to simulate models, yet few simulations have been reported in the literature [5], [6], [7]. A simulation model streamlines the design process, allowing designers to vary parameters and test the results without constructing a prototype and testing in the field.

One study [8] used the inverse-forward dynamics approach to investigate the interaction of the biomechanical system with other technical systems. This study validated the inclination that simulation can help in the design process. Studies have also been conducted for assistive devices. In one such study [9], the authors analyzed trajectories of hip and ankle joints from cubic spine interpolation coupled with geometry and motion restraints to develop a parameterized model of the body's walking pattern. Comparing simulation and experimental results, it was concluded that simulation can achieve adequate results. Motivated by the potential applications of prosthesis simulation, this paper attempts to fill in a gap in the literature by demonstrating a simulation of a human with a transfemoral prosthesis.

Constructing the simulations of interest in this paper issues another interesting challenge: "human controllers" must be designed with the capability of mimicking a human gait. To construct such controllers, this paper analyzes the results of a human walking experiment conducted using the Phase Space System [10] which performed high-frequency motion capture. The study of human walking requires research in either robotics and control or biomechanics. In the context of biomechanics, researchers are often interested in forces and dynamics [11], [12]; specifically, forces and loading have been studied at the foot [13], [14] and at the hip [15], [16]. Such analysis is useful in the design of prostheses and hip replacements yet fails to give a complete picture of human walking. While many studies have been conducted in the context of biomechanics [17], few have been done with respect to control engineering [18], [19]. When studying the biomechanics of walking, researchers use force plates and force loading models to measure and estimate the distribution of musculoskeletal forces and ground reaction forces [20]. This is used with either inverse-dynamic models [21], [22] or forward-dynamic models [23], [24], [25]. In this paper, we prefer to analyze functions representing outputs on the kinematics of a human. Recent methods have been developed [26], [27] which draw from human data to obtain walking in robotic models. This paper uses methods from [27] to develop the human functions and controllers and achieve simulated walking for a human with prosthesis.

In order to faithfully represent human walking, a human walking experiment is considered [28]. Controllers are designed using simple mathematical functions which attempt to represent the fundamental behaviors of human walking during a walking gait; a state-based parameterization is introduced to remove the time-dependence from these functions. Then, a model of healthy human walking is considered; controllers are created using feedback linearization [29, ch. 9] to achieve humanlike walking on this model; indeed, a simulation shows stable walking. This walking will require large joint velocities, yet recent results have built upon the methods used in this paper to achieve a hybrid zero dynamics which significantly reduces maximum joint velocities [30], [31].

After demonstrating healthy human walking, another model is created with a prosthesis; PD control is used to

Texas A&M University, Department of Mechanical Engineering, 3123 TAMU, College Station, TX 77843-3123, e-mail: {rsinnet,huihuazhao,aames}@tamu.edu

R. W. Sinnet is an NSF Graduate Research Fellow. This work is also supported by NSF grant CNS-0953823 and NHARP award 00512-0184-2009.

mimic the desired human behavior on the prosthetic knee and feedback linearization is used to control the human joints. Simulations using mass, length, and walking data from four different human test subjects were conducted. Each model was made to walk with a prosthesis in simulation without changing any of the parameters characterizing the human behavior. This result signifies that human-inspired control can be used reproduce robustness similar to that of a human.

II. HYBRID SYSTEMS AND ROBOTIC MODELS

Bipedal walking exhibits both discrete and continuous behaviors; it is, therefore, natural to model bipeds as hybrid systems. The point-foot robotic model of a human with a transfemoral prosthesis considered in this paper motivates the use of a two-domain hybrid system—one domain for standing on the human leg and one for standing on the prosthesis. The system evolves in a continuous fashion according to a dynamic model derived from a Lagrangian modeling the mechanical system on each domain. At some point during the gait, the swing foot will strike the ground; this will cause an impact resulting in discrete changes in velocity. This combination of continuous and discrete phenomena is the fundamental concept underlying hybrid systems.

This section formally introduces hybrid systems and discusses how the dynamic model of a robot together with a temporal ordering of discrete events completely determines the hybrid model of a system.

A. Formal Definition of Hybrid Systems

Hybrid systems or *systems with impulse effects* [32] have been studied extensively in a wide variety of contexts and have been used to model a wide range of bipedal robotic systems [33]. In this section, a definition of hybrid systems applicable to bipedal walking is introduced. The gait for the model posed in this paper has two domains with a temporal ordering of discrete events, motivating the application of multi-domain hybrid systems in which the domain graph is a *directed cycle*.

Definition 1: A *directed cycle* is a graph $\Gamma = (V, E)$, with V a set of vertices and E a set of edges—for an edge $e \in E$, denote the source by $\mathrm{sor}(e)$ and the target by $\mathrm{tar}(e)$—in which the edges and vertices can be written

$$V = \{v_1, v_2, \dots, v_p\}, \tag{1}$$
$$E = \{e_1 = \{v_1, v_2\}, e_2 = \{v_2, v_3\}, \dots, e_p = \{v_p, v_1\}\},$$

where p is the number of discrete domains in the corresponding hybrid model. This is now illustrated with an example:

Example 1: The *domain breakdown* pictured in Fig. 1 has an underlying graph that is a directed cycle; the graph is given by $\Gamma_u = (V_u, E_u)$. In particular, there are two vertices and two edges with

$$V_u = \{HU, PR\},$$
$$E_u = \{\{HU, PR\}, \{PR, HU\}\}$$

With this notion of a directed cycle in hand, the formulation of a hybrid system that is of interest in this paper is now introduced.

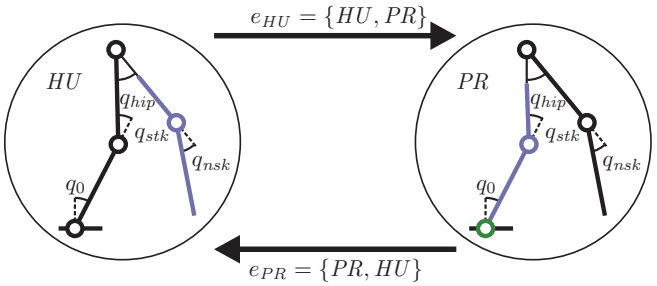

Fig. 1: Domain graph for human with prosthesis model. Circles represent joints with given relative coordinates. Black represents human control, blue indicates prosthesis control, and green indicates no actuation.

Definition 2: A *hybrid control system in a cycle* is a tuple,

$$\mathscr{HC} = (\Gamma, \mathcal{D}, U, S, \Delta, FG),$$

where

- $\Gamma = (V, E)$ is a *directed cycle*,
- $\mathcal{D} = \{\mathcal{D}_v\}_{v \in V}$ is a set of *domains of admissibility* with $\mathcal{D}_v \subseteq \mathcal{X}_v \times U_v$ a smooth submanifold, where $\mathcal{X}_v$ represents the state space of the system,
- $U = \{U_v\}_{v \in V}$ with $U_v \subseteq \mathbb{R}^{m_v}$ a set of admissible controls,
- $S = \{S_e\}_{e \in E}$ is a set of *guards* or *switching surfaces*, with $S_e \subseteq \mathcal{D}_{\mathrm{sor}(e)}$,
- $\Delta = \{\Delta_e\}_{e \in E}$ is a set of *reset maps*, with $\Delta_e : S_e \to \mathcal{D}_{\mathrm{tar}(e)}$ a smooth map,
- $FG = \{(f_v, g_v)\}_{v \in E}$ with (f_v, g_v) a *control system* on D_v, i.e., $\dot{x} = f_v(x) + g_v(x)u \ \forall \ (x^T, u^T)^T \in \mathcal{D}_v$.

A *hybrid system* is a hybrid control system with $U_v = \emptyset \ \forall \ v \in V$, e.g., any applicable feedback controllers have been applied, making the system closed-loop. In this case,

$$\mathscr{H} = (\Gamma, \mathcal{D}, S, \Delta, F),$$

where $F = \{f_v\}_{v \in E}$, with f_v a *dynamical system* on $\mathcal{X} \subseteq \mathcal{D}_v$, i.e., $\dot{x} = f_v(x)$.

Hybrid Period Orbits and the Poincaré Map. In order to establish the stability of hybrid periodic orbits, the standard technique of studying the corresponding Poincaré map [34] is used. In particular, taking S_v for an arbitrary domain v to be the Poincaré section, one obtains the Poincaré map, $\mathcal{P} : S_v \to S_v$, which maps from a point on the guard to a point on the guard. Let x^* be a fixed point of $\mathcal{P}$. Then, a hybrid periodic orbit $\mathcal{O}$ with $x^* \in \mathcal{O}$ is locally exponentially stable if and only if P is locally exponentially stable (as a discrete-time dynamical system, $z_{i+1} = P(z_i)$). Although it is not possible to explicitly compute the Poincaré map, one can compute a numerical approximation of this map through simulation and thereby test its stability numerically. This gives a concrete method for practically testing the stability of hybrid periodic orbits.

B. Constructing Hybrid Systems

It will now be shown how to construct a hybrid system using a Lagrangian and discrete events—the feet periodically

strike the ground. Begin with the assumption that the stance foot is pinned to the ground and use this to describe the continuous dynamics. In order to derive the discrete dynamics, one must introduce additional Cartesian coordinates p_x, p_z at the stance foot. A more general discussion factoring in ground wrenches and applicable to a wider range of bipeds can be found in [33].

Domain and Guard. The domain specifies the allowable configuration of the system. For a biped, the feet must be above (or in contact with) the ground at all times. This condition is specified by a unilateral constraint, h, which is the height of the swing foot; this naturally leads to a definition for the domain:

$$\mathcal{D} = \left\{(q^T, \dot{q}^T)^T \in T\mathcal{Q} : h(q) \geq 0\right\}. \tag{2}$$

The guard is just the boundary of the domain with the additional assumption that the unilateral constraint is decreasing, i.e., the vector field is pointed outside of the domain, or

$$S = \left\{(q^T, \dot{q}^T)^T \in T\mathcal{Q} : h(q) = 0 \text{ and } \frac{\partial h(q)}{\partial q}\,\dot{q} < 0\right\}. \tag{3}$$

Continuous Dynamics. The Lagrangian of a robot, $\mathcal{L} : T\mathcal{Q} \to \mathbb{R}$, can be stated in terms of its kinetic energy, $K : T\mathcal{Q} \to \mathbb{R}$, and its potential energy, $V : \mathcal{Q} \to \mathbb{R}$, as $\mathcal{L}(q, \dot{q}) = K(q, \dot{q}) - V(q)$. The Euler-Lagrange equation gives the dynamic model, which, for robotic systems (see [35]), is stated as:

$$D(q)\,\ddot{q} + H(q, \dot{q}) = B(q)\,u \tag{4}$$

with inertia map $D(q)$ and torque distribution map $B(q)$, and

$$H(q, \dot{q}) = C(q, \dot{q})\,\dot{q} + G(q)$$

containing terms resulting from the Coriolis effect and gravity; $C(q, \dot{q})$ can be found using standard methods [35]. Manipulation of (4) leads to the control system (f, g):

$$f(q, \dot{q}) = \begin{bmatrix} \dot{q} \\ -D^{-1}(q)H(q, \dot{q}) \end{bmatrix},\ g(q) = \begin{bmatrix} \mathbf{0} \\ D^{-1}(q)B(q) \end{bmatrix}. \tag{5}$$

Discrete Dynamics. In order to define the reset map, it is necessary to first augment the configuration space $\mathcal{Q}$. Attach a frame R_e to the stance foot; let w represent the Cartesian position of R_e in the xz-plane. The *generalized coordinates* are then written

$$q_e = (p_x, p_z, q^T)^T \in \mathcal{Q}_e = \mathbb{R}^2 \times \mathcal{Q}.$$

Without loss of generality, assume that the values of the extended coordinates are zero throughout the gait. Moreover, the configuration variable does not change through impact so these values will be zero right after impact. Therefore, introduce the embedding $\iota : \mathcal{Q} \to \mathcal{Q}_e$ defined as $(0, 0, q) \mapsto q_e$; this allows the generalized coordinates to be written in terms of the shape coordinates.

The impact model used is [36]; plastic rigid-body impacts with impulsive forces are used to simulate impact. Impulsive forces can be applied to the swing foot when it contacts the ground; this is representable as the holonomic constraint $J(q)\,\dot{q} = (v_x, v_z)^T$ where v_x and v_z are the x and z velocities, respectively, of the frame R_e. The *impact map* gives the post-impact velocity (see [37]):

$$\dot{q}^+ = P(q_e, \dot{q}_e^-) = \tag{6}$$
$$(I - D^{-1}(q_e)J^T(q_e)(J(q_e)D^{-1}(q_e)J(q_e))^{-1}J(q_e))\,\dot{q}_e^-$$

with I the identity matrix.

In the bipedal walking literature, it is common to use a stance/swing notation for the legs [32]; it can be more intuitive to think of control design for the legs in the context of stance/swing than left/right—the differences in behavior provide a natural way of transforming the design problem. To achieve this, the legs must be "swapped" at impact. A coordinate transformation $\mathcal{R}$ (i.e., a *state relabeling procedure*) switches the roles of the left and right legs:

$$\Delta(q, \dot{q}) = \begin{bmatrix} \mathcal{R} & \mathbf{0} \\ \mathbf{0} & \mathcal{R} \end{bmatrix} \begin{bmatrix} \pi \circ \iota(q) \\ \pi^* \circ P(\iota(q), \iota^*(\dot{q})) \end{bmatrix}, \tag{7}$$

where $\iota^* : T\mathcal{Q} \to T\mathcal{Q}_e$ is the pushforward of $\iota : \mathcal{Q} \to \mathcal{Q}_e$ and $\pi : \mathcal{Q}_e \to \mathcal{Q}$ is the canonical projection associated to ι with pushforward $\pi^* : T\mathcal{Q}_e \to T\mathcal{Q}$. The reset map (7) takes a point on the guard and maps it to the domain (2).

C. Bipedal Models

In this paper, two models are considered: mainly, the paper focuses on a human with a prosthesis, however, also considered for the sake of comparison is a model of human without a prosthesis. Both models have the same mass and length distribution, so the construction will be similar; the few differences will be pointed out during construction. The physical model has knees and assumes point-masses for simplicity. There are five point masses: one for the hip, one for each thigh, and one for each calf; the values of the masses are calculated using a weight distribution [12] for each test subject in Fig. 2(b). The masses and lengths are depicted in Fig. 2(a) with the values given in Fig. 2(b). The model also has point feet but some clarification will be given shortly. Recall that the goal of this paper is to simulate prosthetic walking. Specifically, a transfemoral prosthesis with only one actuator at the knee is under consideration.

Fig. 2: Physical configuration of the human/prosthesis model.

(a) Bipedal model.

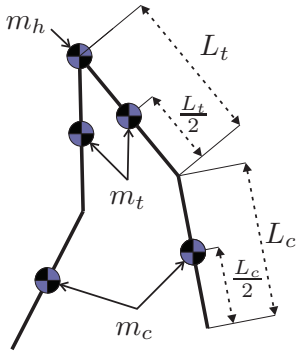

(b) Subject and model parameters.

Var.	S1	S2	S3	S4
Sex	M	F	F	M
Age	22	23	19	30
Ht. (cm)	169.5	165.5	163.5	170.0
Wt. (kg)	90.7	47.6	53.6	69.1
m_h (kg)	61.5	32.3	32.3	36.3
m_t (kg)	9.1	4.8	4.8	5.4
m_c (kg)	5.5	2.9	2.9	3.3
L_t (cm)	40.1	39.2	39.2	40.3
L_c (cm)	43.6	37.6	37.6	38.1

The healthy human model has symmetric walking and thus assumes a one-domain hybrid system, i.e., the one vertex in the graph is connected to itself whereas the asymmetry of the prosthetic model motivates the use of a two-domain hybrid system. Denote the domains or phases for the prosthetic model by HU and PR, representing the two distinct phases when the model is standing on the human leg or standing on the prosthetic leg, respectively. To simplify the model, point feet are assumed, yet full control authority at the stance foot is granted for a model when it is standing on the human leg. Thus, the human model has full control authority throughout the gait and the prosthetic model has full control authority only in domain HU, meaning underactuation of the prosthetic ankle; see Fig. 1.

Hybrid Model Construction. Let the human and prosthetic models be represented by labels H and P, respectively. The construction of the hybrid control systems

$$\mathscr{HC}_H = (\Gamma^H, \mathcal{D}^H, U^H, S^H, \Delta^H, \mathcal{FG}^H),$$
$$\mathscr{HC}_P = (\Gamma^P, \mathcal{D}^P, U^P, S^P, \Delta^P, \mathcal{FG}^P)$$

will now be given. The human model is a simple hybrid system with one domain; the prosthesis model has two domains—the graph Γ^P is shown in Fig. 1 and given explicitly in Example 1. The shape coordinates comprise the configuration space for both models:

$$q = (q_0^T, q_{stk}^T, q_{hip}^T, q_{swk}^T)^T \in \mathcal{Q}.$$

For the human model, full control authority is granted so $U^H = \mathbb{R}^4$, and, as mentioned earlier, control authority on q_0 is granted only in domain HU for the prosthesis; thus, the admissible control is $U^P = \{U_{HU}, U_{PR}\}$ with $U_{HU} \subseteq \mathbb{R}^4$ and $U_{PR} \subseteq \mathbb{R}^3$, as depicted in Fig. 1. For both models, the guard and domain can be determined from the unilateral constraint h, which represents the height of the swing foot above the ground. Then, the domains for both the human model and the prosthesis model (for domains HU and PR) are $\mathcal{D}^H$ and $\mathcal{D}^P = \{\mathcal{D}^P_{HU}, \mathcal{D}^P_{PR}\}$ and the guards are S^H and $S^P = \{S^P_{HU}, S^P_{PR}\}$, respectively; the elements $\mathcal{D}^H = \mathcal{D}^P_{HU} = \mathcal{D}^P_{PR}$ and $S^H = S^P_{HU} = S^P_{PR}$ are equivalent and are given by (2) and (3), respectively.

The Lagrangian is determined using standard methods [35]; then, the Euler-Lagrange equation determines the dynamic model on each domain as in (4). For the two domains of the model in this paper, control systems $\mathcal{FG}_H = (f_H, g_H)$ and $\mathcal{FG}_{P,HU} = (f_{P,HU}, g_{P,HU})$ and $\mathcal{FG}_{P,PR} = (f_{P,PR}, g_{P,PR})$ for the set $\mathcal{FG}_P = \{\mathcal{FG}_{P,HU}, \mathcal{FG}_{P,PR}\}$ are given by (5). Finally, the elements of the reset maps Δ^H and $\Delta^P = \{\Delta^P_{HU}, \Delta^P_{PR}\}$ are given by (7) and, under the assumptions that the biped is physically symmetric and that the acuators do not produce impulsive torques, are equivalent, i.e., $\Delta^H = \Delta^P_{HU} = \Delta^P_{PR}$.

III. HUMAN WALKING CONTROLLERS

The controller design process hinges on the goal of designing humanlike walking using experimentally-collected human walking data [28]. The experiment will be described and the resulting data will be examined to identity fundamental human walking behaviors; these behaviors will be represented as mathematical functions on the kinematics of the human. Feedback linearization [29, ch. 9] will be used to design controllers for human and human/prosthesis models which will impose these human behaviors.

Human Walking Experiment. An experiment was performed using the Phase Space System [10] which provided position data of sensors on human test subjects at a rate of 480 Hz and an accuracy of one millimeter. Nine subjects were measured, eight trials each, walking approximately three full steps per trial. The data for each subject were averaged to obtain smooth trajectories for all nine subjects. In this paper, four of these subjects are considered.

Characterizing Human Behavior. Analysis of the data indicates that four behaviors represent the human gait inasmuch as the model of interest is relatively simple, having only four links. The behaviors are the angles of both knees, the slope of the swing leg, and the forward position of the hip. The human functions which model these behaviors are given in Table I; an optimization problem can be solved to characterize the walking in terms of the functions for a given test subject. These human functions are central to this paper and the associated body of work [27], [30], [31], [38].

Function Fitting. Consider applying the human functions in Table I to the human data to model the behaviors described. Formally, one seeks the parameters $\{a_i\}$ which minimize the error between the fit and the data; this is expressed mathematically as the optimization problem

$$\min_{\{a_i\}} \sum_{k=1}^{K} (y_d(\tau[k], \{a_i\}) - x[k])^2, \tag{8}$$

TABLE I: Table containing parameter values of our constraint functions for the four test subjects. Here, $p_{hip}, m_{nsl}, \theta_{stk}$, and θ_{nsk} are hip x position, non-stance slope, stance knee angle and non-stance knee angle respectively. The first three functions for each subject use the first equation while the last function uses the second equation.

$$y^{\{1,2,3\}} = \frac{a_1 \cos(a_2 t + a_3) + a_4 \sin(a_2 t + a_3)}{e^{a_5 t}} + a_6 t + a_7$$
$$y^4 = a_1 \exp\left(\frac{-(t-a_2)^2}{2(a_3)^2}\right) + a_4$$

S.	Fun.	a_1	a_2	a_3	a_4	a_5	a_6	a_7	Cor.
1	p_{hip}	0	0	0	0	0	1.177	0.705	0.999
	m_{swl}	0	7.461	-2.453	-0.405	0	0	-0.119	0.999
	θ_{stk}	0.083	13.326	0	2.503	4.155	0	-0.257	0.993
	θ_{swk}	-1.015	0.243	0.119	-0.149				0.993
2	p_{hip}	0	0	0	0	0	1.192	0.713	0.998
	m_{swl}	0	6.879	-2.388	-0.485	0	0	-0.068	0.999
	θ_{stk}	0.194	16.153	0	0.384	4.99	0	-0.380	0.956
	θ_{swk}	-1.041	0.239	0.137	-0.184				0.989
3	p_{hip}	0	0	0	0	0	1.532	0.739	0.999
	m_{swl}	0	8.470	-2.109	-0.424	0	0	-0.112	0.999
	θ_{stk}	0.045	16.738	0	0.894	2.255	0	-0.378	0.986
	θ_{swk}	-0.965	0.179	0.119	-0.274				0.993
4	p_{hip}	0	0	0	0	0	0.946	0.538	0.999
	m_{swl}	0	7.0473	-2.476	-0.404	0	0	-0.157	0.999
	θ_{stk}	0.080	13.379	0	1.081	1.662	0	-0.219	0.981
	θ_{swk}	-1.062	0.259	0.131	-0.116				0.995

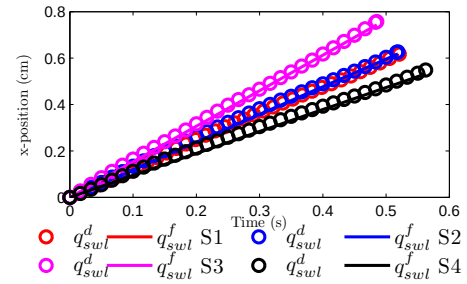

(a) Functions—hip position.

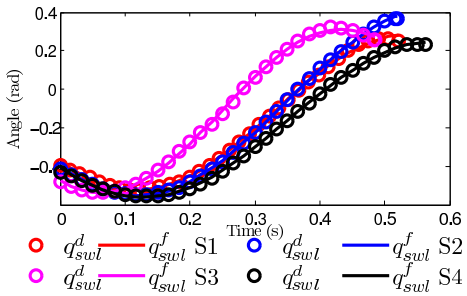

(b) Functions—swing leg slope.

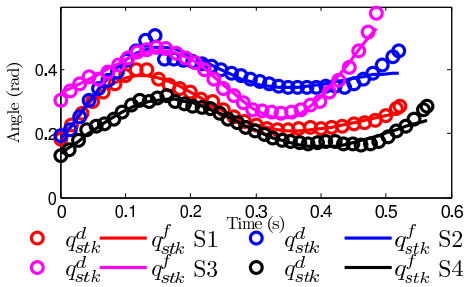

(c) Functions—stance knee angle.

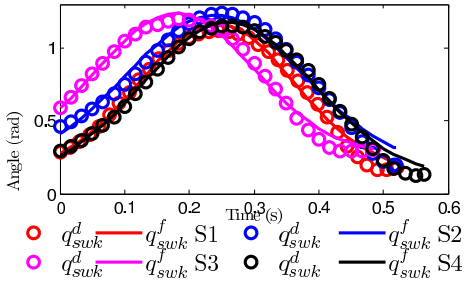

(d) Functions—swing knee angle.

Fig. 3: Plots of the fitted functions and the human data.

where $\tau[k]$ and $x[k]$ represent the time and human data, respectively, with $k \in [1, \dots, K] \subset \mathbb{Z}$ an index for the K data points, and $y_d(\cdot)$ the fitting function with parameters $\{a_i\}$. To be clear, $x[k]$ is the value of the kinematics function on the human at data point k. This problem is solved for the four test subjects and the resulting fit parameters along with the coefficients of correlation are given in Table I.

Tracking Human Behavior. Now that the desired behaviors have been classified, control is necessary to mimic these behaviors. In a formal sense, a control law attempting to impose these behaviors should seek to drive $y^a(q) \to y^d(t)$ as $t \to 0$ where $y^a(q)$ and $y^d(t)$ are the actual and desired values of the human functions, respectively; this is achieved using feedback linearization. Note that the desired functions $y^d(t)$ are time-dependent; in general, time-invariant controllers tend to show more robustness to perturbations.

State-Based Parameterization. Motivated by the desire to design *autonomous* or *time-invariant* controllers, a parameterization for time is introduced, as is common in the literature [39], [40]. Denote the parameterization by $\varsigma : Q \to \mathbb{R}_0^+$ where $\mathbb{R}_0^+$ represents time; ideally, $\varsigma(t)$ should be approximately linear, i.e., $\varsigma(t) \approx \alpha t$ for some α. Fig. 3(a) indicates that $p_{hip}^x \approx \bar{v}_{hip} t$ with $\bar{v}_{hip}^x$ the average x velocity of the hip is approximately linear in time, motivating the following parameterization:

$$\varsigma(t) := \frac{p_{hip}^x(q) - p_{hip}^x(q^-)}{\bar{v}_{hip}^x}. \tag{9}$$

A decision is made to track the velocity v_{hip}^x, driving it to a constant, instead of the associated position. The value of this velocity constant should be the parameter $\bar{v}_{hip}^x$ from (9).

Feedback Linearization. Let $y = y^a - y^d$ with y^a the actual values from the kinematics of the model and y^d the desired values from the fitted functions. Without loss of generality, assume an output having mixed relative degree. Group the output functions as

$$y(q, \dot{q}) = (y_1^T(q, \dot{q}), y_2^T(q))^T, \tag{10}$$

where y_1 and y_2 represent the relative degree one and two outputs respectively. The control law which drives $y(q, \dot{q}) \to 0$ is given by

$$u^{FL}(q, \dot{q}) = -\mathcal{A}^{-1}(q, \dot{q}) \left(\begin{bmatrix} 0 \\ L_f L_f y_2(q) \end{bmatrix} + \begin{bmatrix} L_f y_1(q, \dot{q}) \\ 2\varepsilon L_f y_2(q, \dot{q}) \end{bmatrix} + \begin{bmatrix} \varepsilon\, y_1(q, \dot{q}) \\ \varepsilon^2\, y_2(q) \end{bmatrix} \right), \tag{11}$$

with control gain ε, $L_f y = \frac{\partial y}{\partial x} f(x)$ representing Lie derivatives, and decoupling matrix $A(q)$ given by

$$\mathcal{A}(q, \dot{q}) = \begin{bmatrix} L_g y_1(q, \dot{q}) \\ L_g L_f y_2(q, \dot{q}) \end{bmatrix}$$

for a given control system (f, g).

Human Control. Using the method of feedback linearization as just described, it is possible to explicitly construct a hybrid system modeling healthy human walking. Denote by y^H (with the form of (10)) the output functions to be zeroed as described previously. Then, the control law which drives $y^H \to 0$ as $t \to 0$ is written $u^H(q, \dot{q})$ and given in (11). This control is applied to the control system (f_H, g_H) to obtain the closed-loop vector field

$$f_H^{FL}(q, \dot{q}) = f_H(q, \dot{q}) + g_H(q) u^H(q, \dot{q}).$$

Using this new vector field, a hybrid system is constructed modeling healthy human walking:

$$\mathscr{H}_H^{FL} = (\mathcal{D}^H, S^H, \Delta^H, F_H^{FL}), \tag{12}$$

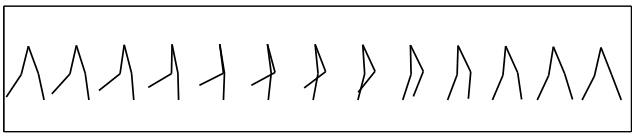

Fig. 4: Simulated gait for healthy human walking, S1. Only one step is shown due to symmetry.

where we have dropped the discrete graph Γ as it is unnecessary for simple hybrid systems (i.e., single-domain hybrid systems).

Simulations. Simulations of the hybrid system (12) were performed for each of the test subjects, S1–S4. Fixed points of the Poincaré map were found; see Fig. 5(a). For a given system, a fixed point indicates an orbit. To show stability of the orbit, one must consider the eigenvalues associated with a Jacobian matrix linearized about a fixed point on the orbit. Eigenvalues for the simulations are shown in Fig. 5(b). These eigenvalues are all less than unity, thus the orbit is locally exponentially stable. In terms of walking, this means that the system exhibits stable walking. The gait for S1 is shown in Fig. 4. The humanlike nature of the walking can be seen in video [41]. The simulations just described show a natural way to model the human control aspect. This will be leveraged when creating the simulation for the human with prosthesis.

IV. DESIGNING HUMAN/PROSTHESIS CONTROLLERS

Having examined healthy human walking, the main interest of this paper can now be explored: simulation of a human with a transfemoral prosthesis. A human function has already been defined representing the behavior of a knee. It will be convenient to use PD control to try to mimic this behavior on the prosthesis. After applying PD control for the prosthesis, the human controllers designed around feedback linearization will be applied; the idea behind this is to let the human controller handle the human actuators on the model.

Prosthesis Control. To achieve the goal of human tracking on the prosthetic knee on both domains, HU and PR, a PD controller is used. Let

$$y_p^{HU}(q) = \theta^a_{swk}(q) - \theta^d_{swk}(\varsigma(q)),$$
$$y_p^{PR}(q) = \theta^a_{stk}(q) - \theta^d_{stk}(\varsigma(q))$$

represent the error in tracking on domains HU and PR, respectively, where θ^a are actual values of the knee angles and θ^d are the desired values as given in Table I. Then, using the parameterization (9), control laws for the prosthesis are

$$u_p^{HU}(q) = k_p^{HU} y_p^{HU}(q) + k_d^{HU} \dot{y}_p^{HU}(q),$$
$$u_p^{PR}(q) = k_p^{PR} y_p^{PR}(q) + k_d^{PR} \dot{y}_p^{PR}(q).$$

The control laws can be applied to the control systems $\mathcal{FG}_{P,HU}$ and $\mathcal{FG}_{P,PR}$ viz.

$$f^{PD}_{P,HU}(q,\dot{q}) = f_{P,HU}(q,\dot{q}) + g^p_{P,HU}(q) u_p^{HU},$$
$$f^{PD}_{P,PR}(q,\dot{q}) = f_{P,PR}(q,\dot{q}) + g^p_{P,PR}(q) u_p^{HU},$$

Var.	P1	P2	P3	P4	H1	H2	H3	H4
q_0	-0.388	-0.422	-0.305	-0.370	-0.366	-0.410	-0.343	-0.326
q_{stk}	0.011	-0.064	-0.174	-0.015	-0.006	-0.066	-0.153	0.014
q_{hip}	-2.521	-2.412	-2.490	-2.477	-2.540	-2.432	-2.362	-2.611
q_{swk}	-0.249	-0.366	-0.387	-0.180	-0.247	-0.366	-0.264	-0.182
$\dot{q}_0$	2.597	14.707	21.433	4.286	3.961	10.904	17.388	1.093
$\dot{q}_{stk}$	-1.854	-20.070	-29.016	-4.624	-3.990	-14.556	-23.598	0.001
$\dot{q}_{hip}$	-0.806	4.857	8.603	-0.089	0.329	3.238	5.925	-0.519
$\dot{q}_{swk}$	-1.344	-2.145	-0.852	-2.631	-0.654	-1.748	-3.221	-0.164

(a) Fixed points for simulated gaits.

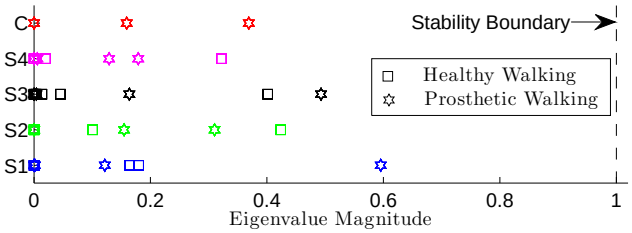

(b) Eigenvalues for healthy and human walking.

Fig. 5: Fixed points and eigenvalues for simulations. S1-4 represent the subjects.

where

$$g^p_{P,HU}(q) = g_{P,HU}(q) \left(\frac{\partial q_{swk}}{\partial q} \right)^T,$$
$$g^p_{P,PR}(q) = g_{P,PR}(q) \left(\frac{\partial q_{stk}}{\partial q} \right)^T.$$

Using these control fields, a new hybrid control system with fields $\mathcal{FG}^{PD}_P = \{\mathcal{FG}^{PD}_{P,HU}, \mathcal{FG}^{PD}_{P,PR}\}$ for $\mathcal{FG}^{PD}_{P,HU} = (f^{PD}_{P,HU}, g_{P,HU})$ and $\mathcal{FG}^{PD}_{P,PR} = (f^{PD}_{P,PR}, g_{P,PR})$ is created:

$$\mathscr{HC}^{PD}_P = (\Gamma^P, \mathcal{D}^P, U^P, S^P, \Delta^P, FG^{PD}_P), \tag{13}$$

Human Control. To implement the controller on each domain, first consider which functions are to be tracked: on both domains, the human knee angle and swing leg slope are tracked. Additionally, on domain HU, the hip velocity is tracked. Under these assumptions, the control fields can be written

$$g^h_{P,HU}(q) = g_{P,HU}(q) \left(\frac{\partial (q_0, q_{stk}, q_{hip})}{\partial q} \right)^T,$$
$$g^h_{P,PR}(q) = g_{P,PR}(q) \left(\frac{\partial (q_{hip}, q_{swk})}{\partial q} \right)^T.$$

Using these control fields with the control laws (11), the closed-loop vector fields $\mathcal{F}_P = \{\mathcal{F}^{PD,FL}_{P,HU}, \mathcal{F}^{PD,FL}_{P,PR}\}$ for $\mathcal{F}^{PD,FL}_{P,HU} = f^{PD,FL}_{P,HU}$ and $\mathcal{F}^{PD,FL}_{P,PR} = f^{PD,FL}_{P,PR}$ can be created:

$$f^{PD,FL}_{P,HU}(q,\dot{q}) = f^{PD}_{P,HU}(q,\dot{q}) + g^h_{P,HU}(q) u^h_{HU},$$
$$f^{PD,FL}_{P,PR}(q,\dot{q}) = f^{PD}_{P,PR}(q,\dot{q}) + g^h_{P,PR}(q) u^h_{PR},$$

The end result is a hybrid system modeling a human with prosthesis:

$$\mathscr{H}^{PD,FL}_P = (\Gamma^P, \mathcal{D}^P, S^P, \Delta^P, F^{PD,FL}_P). \tag{14}$$

Simulations. Simulations of the hybrid system (14) were performed for each of the test subjects, S1–S4. Fixed points

of the Poincaré map were found (Fig. 5(a)) along with eigenvalues (Fig. 5(b)). Like before, these eigenvalues are all less than unity, thus the orbit is locally exponentially stable. In terms of walking, this means that the system exhibits stable walking. The walking can be seen in video [41]. Tiles and phase portraits for each subject's gait are shown in Fig. 6.

Concluding Remarks. The main point behind this paper was to design a simulation capable of testing controlled prostheses. To construct this simulation, a human-inspired model was used with human-inspired controllers making use of human functions. It was found that this simulation could not only accurately reproduce human walking but also exhibited some degree of robustness. The robustness is substantiated by the simplicity of the prosthesis controller design and the stability of the resulting human/prosthesis models. The hope is that, in the future, prosthesis designs can be rapidly tested by changing the prosthesis design or controllers and checking stability in simulation.

REFERENCES

[1] T. R. Dillingham, L. E. Pezzin, and E. J. Mackenzie, "Limb amputation and limb deficiency: epidemiology and recents trends in the United States," *South. Med. J.*, vol. 95, no. 8, pp. 875–883, Aug. 2002.

[2] A. J. Thurston, "Paré and prosthetics: the early history of artificial limbs," *ANZ J. Surgery*, vol. 77, no. 12, pp. 1114–9, Dec. 2007.

[3] C. Dundass, G. Z. Yao, and C. K. Mechefske, "Initial biomechanical analysis and modeling of transfemoral amputee gait," *Prosthetic and Orthotic Science*, vol. 15, no. 1, pp. 20–6, Jan. 2003.

[4] T. Chin, K. Machida, S. Sawamura, R. Shiba, H. Oyabu, Y. Nagakura, I. Takase, and A. Nakagawa, "Comparison of different microprocessor controlled knee joints on the energy consumption during walking in trans-femoral amputees: Intelligent knee prosthesis (ip) versus c-leg," *Prosthetics and Orthotics International*, vol. 30, no. 1, pp. 73–80, Apr. 2006.

[5] K. Ono and M. Katsumata, "Analytical study of active prosthetic legs," *J. of System Design and Dynamics*, vol. 1, no. 3, pp. 548–57, Mar. 2007.

[6] J. K. Rai, R. P. Tewari, and D. Chandra, "Hybrid control strategy for robotic leg prosthesis using artificial gait synthesis," *Int. J. of Biomech. and Biomed. Robots*, vol. 1, no. 1, pp. 44–50, Jan. 2009.

[7] M. F. Eilenberg, H. Geyer, and H. Herr, "Control of a powered ankle-foot prosthesis based on a neuromuscular model," *IEEE Trans. on Neural Systems and Rehabilitation Eng.*, vol. 18, no. 2, pp. 164–73, Apr. 2010.

[8] P. Brugger and H.-B. Schiedmayer, "Simulating prosthetic gait—lessons to learn," *Proc. in Applied Mathematics and Mechanics*, vol. 3, pp. 64–7, Nov. 2003.

[9] L. Wang, Z. Deng, L. Zhang, and Q. Meng, "Analysis of assistant robotic leg on MATLAB," in *IEEE Intl. Conf. on Mechatronics and Automation*, 2006, pp. 1092–6.

[10] http://www.phasespace.com/.

[11] A. Seireg and R. J. Arvikar, "The prediction of muscular load sharing and joint forces in the lower extremities during walking," *J. of Biomech.*, vol. 8, pp. 89–102, Mar. 1975.

[12] D. A. Winter, *Biomechanics and Motor Control of Human Movement*, 2nd ed. New York: Wiley-Interscience, 1990.

[13] S. K. Au, P. Dilworth, and H. Herr, "An ankle-foot emulation system for the study of human walking biomechanics," in *IEEE Intl. Conf. Robotics and Automation*, Orlando, May 2006, pp. 2939–45.

[14] M. M. Rodgers, "Dynamic biomechanics of the normal foot and ankle during walking and running," *Physical Therapy*, vol. 68, no. 12, pp. 1822–30, Dec. 1988.

[15] G. Bergmann, F. Graichen, and A. Rohlmann, "Hip joint loading during walking and running, measured in two patients," *J. of Biomech.*, vol. 26, no. 8, pp. 969–90, Aug. 1993.

[16] M. O. Heller, G. Bergmann, G. Deuretzbacher, L. Dürselen, M. Pohl, L. Claes, N. P. Haas, and G. N. Duda, "Musculo-skeletal loading conditions at the hip during walking and stair climbing," *J. of Biomech.*, vol. 34, no. 1, pp. 883–93, Jul. 2001.

[17] D. H. Sutherland, K. R. Kaufman, and J. R. Moitoza, *Human Walking*, 3rd ed. Baltimore: Lippincott Williams & Wilkins, Dec. 2005, ch. Kinematics of Normal Human Walking, pp. 23–44.

[18] A. G. Bharatkumar, K. E. Daigle, M. G. Pandy, Q. Cai, and J. K. Aggarwal, "Lower limb kinematics of human walking with the medial axis transformation," in *IEEE Workshop on Motion of Non-Rigid and Articulated Objects*, Austin, Nov. 1994, pp. 70–6.

[19] V. M.Zatsiorsky, *Kinematics of Human Motion*, 1st ed. Champaign: Human Kinetics, 1997.

[20] S. H. Scott and D. A. Winter, "Biomechanical model of the human foot: Kinematics and kinetics during the stance phase of walking," *J. of Biomech.*, vol. 26, no. 9, pp. 1091–104, Sep. 1993.

[21] U. Glitsch and W. Baumann, "The three-dimensional determination of internal loads in the lower extremity," *ASME J. of Biomech. Eng.*, vol. 30, no. 11, pp. 1123–31, Nov. 1997.

[22] S. Siegler and W. Liu, *Three-Dimensional Analysis of Human Locomotion*, 1st ed. New York: John Wiley & Sons, 1997, ch. Inverse Dynamics in Human Locomotion, pp. 191–209.

[23] F. C. Anderson and M. G. Pandy, "Dynamic optimization of human walking," *ASME J. of Biomech. Eng.*, vol. 123, no. 5, pp. 381–90, Oct. 2001.

[24] R. R. Neptune, S. A. Kautz, and F. E. Zajac, "Contributions of the individual ankle plantar flexors to support, forward progression and swing initiation during walking," *J. of Biomech.*, vol. 34, no. 11, pp. 1387–98, Nov. 2001.

[25] M. G. Pandy and N. Berme, "A numerical method for simulating the dynamics of human walking," *J. of Biomech.*, vol. 21, no. 12, pp. 1043–51, Apr. 1988.

[26] S. Srinivasan, I. A. Raptis, and E. R. Westervelt, "Low-dimensional sagittal plane model of normal human walking," *ASME J. of Biomech. Eng.*, vol. 130, no. 5, Oct. 2008.

[27] R. W. Sinnet, M. J. Powell, R. P. Shah, and A. D. Ames, "A human-inspired hybrid control approach to bipedal robotic walking," in *18th IFAC World Congress*, Milano, Sep. 2011.

[28] http://www.eecs.berkeley.edu/∼ramv/HybridWalker.

[29] S. S. Sastry, *Nonlinear Systems: Analysis, Stability and Control*. New York: Springer, 1999.

[30] A. D. Ames, R. Vasudevan, and R. Bajcsy, "Human-data based cost of bipedal robotic walking," in *Hybrid Systems: Computation and Control*, Chicago, Apr. 2011, pp. 151–60.

[31] A. D. Ames, "First steps toward automatically generating bipedal robotic walking from human data," in *8th Intl. Workshop on Robot Motion and Control*, Gronów, Jun. 2011.

[32] J. W. Grizzle, G. Abba, and F. Plestan, "Asymptotically stable walking for biped robots: Analysis via systems with impulse effects," *IEEE TAC*, vol. 46, no. 1, pp. 51–64, Jan. 2001.

[33] J. W. Grizzle, C. Chevallereau, A. D. Ames, and R. W. Sinnet, "3D bipedal robotic walking: models, feedback control, and open problems," in *IFAC Symposium on Nonlinear Control Systems*, Bologna, Sep. 2010.

[34] B. Morris and J. W. Grizzle, "A restricted Poincaré map for determining exponentially stable periodic orbits in systems with impulse effects: Application to bipedal robots," in *44th IEEE Conf. on Decision and Control and European Control Conf.*, Sevilla, Dec. 2005.

[35] R. M. Murray, Z. Li, and S. S. Sastry, *A Mathematical Introduction to Robotic Manipulation*. Boca Raton: CRC Press, 1994.

[36] Y. Hürmüzlü and D. B. Marghitu, "Rigid body collions of planar kinematic chains with multiple contact points," *Intl. J. of Robotics Research*, vol. 13, no. 1, pp. 82–92, Feb. 1994.

[37] R. W. Sinnet and A. D. Ames, "2D bipedal walking with knees and feet: A hybrid control approach," in *Joint 48th IEEE Conf. on Decision and Control and 28th Chinese Control Conf.*, Shanghai, Dec. 2009, pp. 3200–7.

[38] R. W. Sinnet, M. J. Powell, S. Jiang, and A. D. Ames, "Compass gait revisited: A human data perspective with extensions to three dimensions," in *50th IEEE Conf. on Decision and Control and European Control Conf.*, Orlando, Dec. 2005.

[39] E. R. Westervelt, J. W. Grizzle, and D. E. Koditschek, "Hybrid zero dynamics of planar biped walkers," *IEEE TAC*, vol. 48, no. 1, pp. 42–56, Jan. 2003.

[40] E. R. Westervelt, J. W. Grizzle, C. Chevallereau, J. H. Choi, and B. Morris, *Feedback Control of Dynamic Bipedal Robot Locomotion*. Boca Raton: CRC Press, 2007.

[41] http://www.youtube.com/user/ProfAmes/.

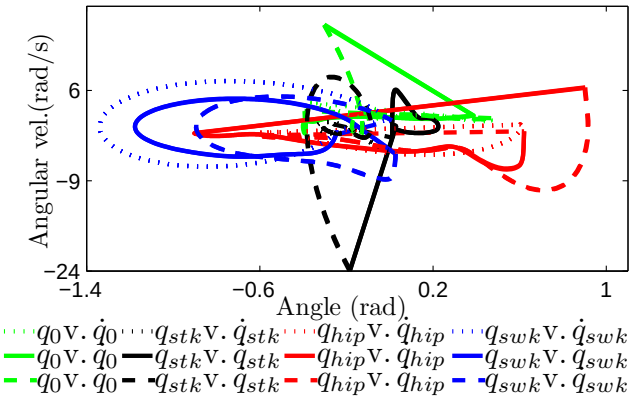

(a) S1—Phase portrait.

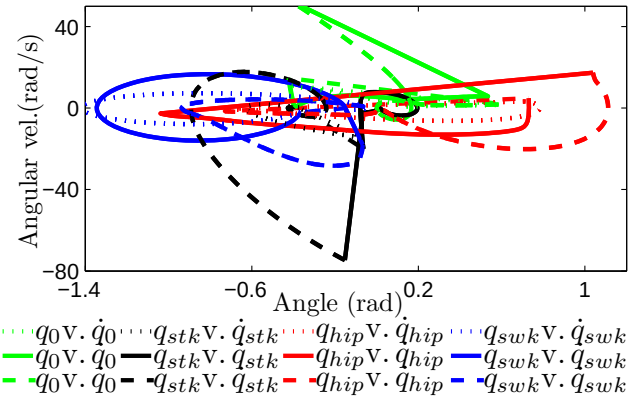

(b) S2—Phase portrait.

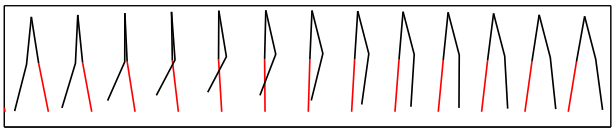

(c) S1—Human stance leg, prosthesis swing leg.

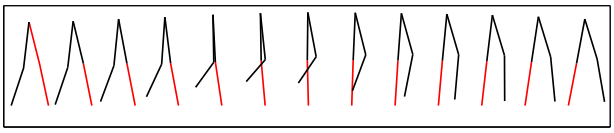

(d) S2—Human stance leg, prosthesis swing leg.

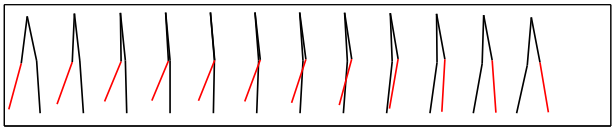

(e) S1—Prosthesis stance leg, human swing leg.

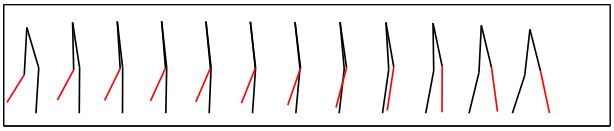

(f) S2—Prosthesis stance leg, human swing leg.

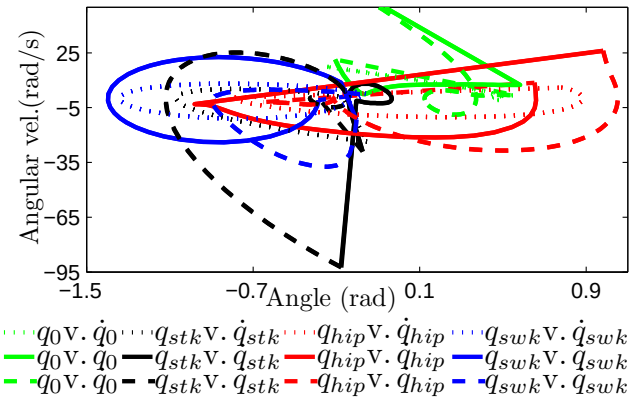

(g) S3—Phase portrait.

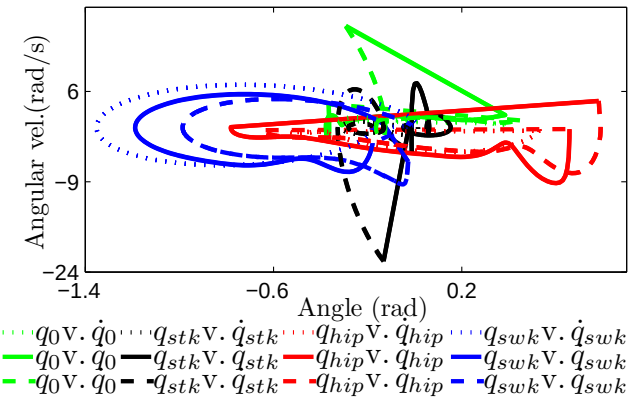

(h) S4—Phase portrait.

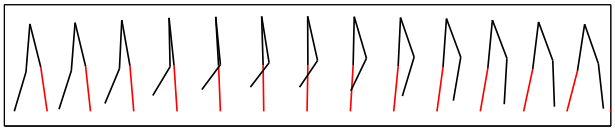

(i) S3—Human stance leg, prosthesis swing leg.

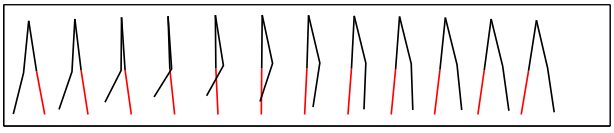

(j) S4—Human stance leg, prosthesis swing leg.

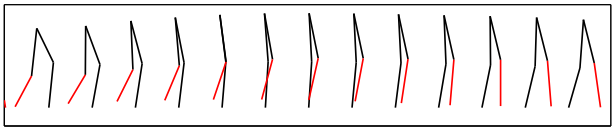

(k) S3—Prosthesis stance leg, human swing leg.

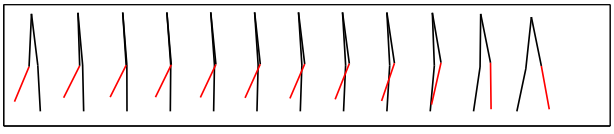

(l) S4—Prosthesis stance leg, human swing leg.

Fig. 6: Outputs and phase portraits for simulations. The top walking tiles in each set represent domain HU and the bottom walking tiles represent domain PR. The red leg is the prosthesis.